Reprocessable and Recyclable Polymer Network Electrolytes via Incorporation of Dynamic Covalent Bonds

Yangju Lin, Yuelang Chen, Zhiao Yu, Zhuojun Huang, Jian-Cheng Lai, Jeffrey B.-H. Tok, Yi Cui, and Zhenan Bao*

ABSTRACT: Mechanically durable polymer network electrolytes are desirable for batteries; however, covalent cross-linking adversely affects their large-scale manufacturing, and they are difficult to recycle post-lifespan. Here, we address the electrolyte reprocessability and recyclability challenges through the use of dynamic covalent bonds for polymer network solid electrolytes. Specifically, the associative dynamic vinylogous urethane motif is incorporated into a poly(ethylene oxide) network electrolyte containing lithium bis(fluorosulfonyl)imide (LiFSI) salt. The resulting dynamic covalent network electrolyte possesses a modest ion conductivity (~10^{-5} S/cm at room temperature) and good reprocessability. Stress–relaxation studies indicate that the LiFSI salt can catalyze the bond exchange and enhance the network dynamics. Furthermore, the reprocessability associated with bond exchange can be tuned by simply adjusting the formulation of reagent compositions, in which increasing the amount of excess amine or using a shorter chain of PEO prepolymer can further enhance the network dynamics and corresponding reprocessability.

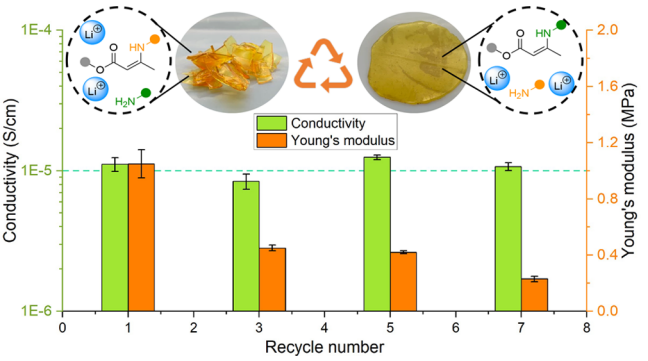

INTRODUCTION

For safer next-generation lithium-ion batteries (LIBs), solid-state electrolytes (including polymer and inorganic electrolytes) have been extensively explored as alternatives to the conventionally flammable and toxic liquid electrolytes.[1] Compared to inorganic electrolytes, polymer electrolytes have attractive features, such as amendable synthesis, low density (i.e., lighter weight per unit volume), compatibility with scalable manufacturing procedures, and good interfacial contact with rigid electrodes owing to their soft nature.[2−4]

Since the seminal work on the complexation behavior of the poly(ethylene oxide) (PEO) backbone with alkaline metal ions by Wright and co-workers,[5] polymer electrolytes comprised of various backbones[6] and architectures[7,8] have been reported. However, it remains a major challenge to achieve high room-temperature ionic conductivity (>10^{-3} S/cm) for practical battery application without volatile flammable solvent additives.[9,10] Currently, PEO-based polymer electrolytes remain among the most ion-conductive polymer electrolytes.[11] Recent simulation investigations suggested that the abundance and connectivity of solvation sites in PEO electrolyte contributed to its high ionic conductivity.[12]

In addition to being ionically conductive, polymer electrolytes also need to be mechanically durable so that they can act as both electrolyte and separator. In this regard, linear and non-cross-linked composite polymer electrolytes may potentially lose dimensional stability and result in a short circuit at elevated temperature. However, most all-solid-state batteries utilizing polymer electrolytes reported to date need to be operated at elevated temperatures (due to their relatively low room-temperature ionic conductivity) and under stack pressure. Chemical cross-linking strategies have generally been applied to ensure desirable mechanical properties. Unfortunately, the resulting polymer cannot be reprocessed as the chemistries used were not designed for this purpose. For compatibility with current manufacturing methods (e.g., roll-to-roll assembly process and hot pressing procedure) for large-scale production of all-solid-state batteries[13] and future sustainability considerations, it is highly desirable that the polymer reprocessabilities be preserved. Furthermore, the battery recycling post-lifespan has attracted increasing attention, and polymer electrolytes also need to be properly recycled to avoid environmental issues associated with plastic[14] and lithium-ion[15] pollution.

There has been significant recent progress in recyclable polymer networks, in which dynamic covalent bonds were incorporated into the network to enable chain exchanges under external stimuli.[16−18] These dynamic covalent networks have been demonstrated to possess both excellent mechanical properties and recyclability. Previous studies have demonstrated the utility of dynamic covalent bonds in polymer network electrolytes,[19−24] while the primary focus in those studies has been on the self-healing properties of polymer electrolyte (Figure S15).[21−24] To date, the only report to achieve recyclable electrolyte was reported by Evans and coworkers, who demonstrated the recycling through disassembly of a network comprised of boronic acid cross-linked triethylene glycol.[19] However, the network ionic conductivity (~10^{-6} S/cm at 25 °C) still needed to be improved, and the intrinsic instability of boronic ester to moisture may be of potential concern. Herein, network electrolytes with stable dimension and direct reprocessing and recycling capabilities will be desirable (and practical) for current manufacturing procedures.

It has been demonstrated that dynamic covalent networks based on associative dynamic covalent bonds (or also known as vitrimer) are able to maintain a constant cross-linking density during the exchange process, providing high dimensional stability.[25,26] Among the various reported associative dynamic covalent bonds, we identified vinyloguous urethane dynamic bonds to be easily accessible through condensation of amine and acetoacetate groups (Figure 1a), and the acetoacetate substrate can be prepared in large quantity using a transesterification procedure[27,28] or copolymerization strategy.[29−31] Therefore, dynamic vinylogous urethane bonds will be a suitable candidate for investigating the use of dynamic covalent polymer networks for direct reprocessable and recyclable cross-linked polymer electrolytes.

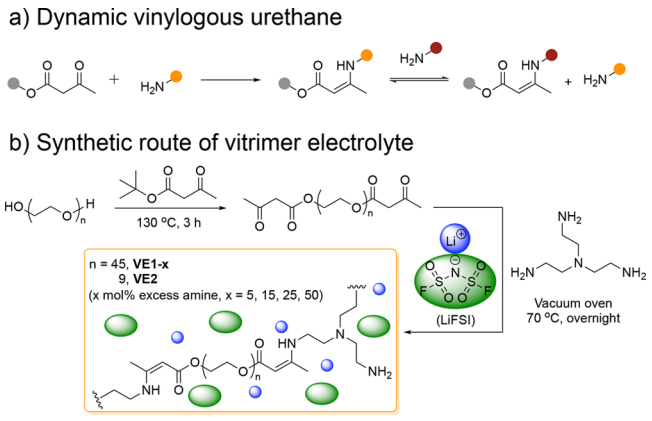

Figure 1. (a) Dynamic exchange of vinylogous urethane with amine and (b) schematic preparation of vitrimer electrolyte.

EXPERIMENTAL SECTION

Materials. Poly(ethylene oxide) (PEO, M_n = 400, 2000), poly(ethylene oxide) methyl ether (mPEO, M_n = 2000), *tert*-butyl acetoacetate, chloroform-*d* ($CDCl_3$), and tetrahydrofuran (THF) were purchased from Sigma-Aldrich. Tris(2-aminoethyl)amine (TAEA) and lithium bis(fluorosulfonyl)imide (LiFSI) were obtained from TCI America. All chemicals were used without further purification.

Synthesis of PEO-AA Prepolymer. PEO polymer (10 g, M_n = 400 or 2000) was weighed in a 100 mL round-bottom flask. A stir bar was then added to the flask, and the polymer was heated at 70 °C and dried under high vacuum overnight. *tert*-Butyl acetoacetate (2.5 equiv for M_n = 400 and 4.0 equiv for M_n = 2000) was added in one portion, and the resulting mixture was heated at 130 °C for 3 h, after which the conversion of the chain end hydroxy group was confirmed by ^{1}H NMR. The excess amount of *tert*-butyl acetoacetate was removed by vacuum distillation. The final product, PEO acetoacetate (PEO-AA), was obtained as a pale brown solid. The conversion was estimated from the ^{1}H NMR spectrum: 4 × 44/190 × 100% = 93% (Figure S1).

Fabrication of Vitrimer Electrolytes. In a typical procedure of vitrimer electrolyte fabrication, acetoacetate terminated PEO polymer (224 mg, ~0.1 mmol) was dissolved in 2 mL of THF in a 20 mL scintillation vial, and LiFSI salt solution in THF (with corresponding lithium salt to ethylene oxide ratio of various values of Li^+/EO = 0.025, 0.05, 0.0625, 0.1, 0.167) was added (Table S1). Subsequently, TAEA (with the 5 mol % excess amine relative to the acetoacetate group) was added to the mixture and further mixed. The resulting solution was then condensed and poured onto a silicon wafer or a Teflon mold. After being heated at 70 °C in a vacuum oven overnight, a yellow vitrimer electrolyte network was obtained. Vitrimer electrolytes (Li^+/EO = 0.0625) with various amounts of excess amine (5, 15, 25, and 50 mol %) were prepared by adjusting the molar ratio of added TAEA (Table S2).

Hot Pressing of Vitrimer Electrolytes. The hot press procedure was conducted using a Dulytek DM1005 clamshell manual rosin heat press. Vitrimer electrolyte samples were sandwiched between 100 μm PFTE sheets and placed between the heating plates. The heating plates were then compressed through the manual screw setup, and the plate temperature was set to 90 °C. After heating for 30 min, a homogeneous film was obtained. The film was then cut into rectangle strips to perform the tensile test. The thickness of the film was controlled by using steel spacers. For EIS measurement, the film thickness was controlled using a 250 μm stainless steel spacer or measured before the test. For the stress−relaxation test, the film thickness was controlled using a 1 mm stainless steel spacer and cut into a disk with diameter of 8 mm using a puncher.

Fabrication of Coin Cells. The vitrimer electrolyte film was punched into a disc using a puncher (diameter of 5/8 in.) and sandwiched between two stainless steel spacers, and the trilayer set was crimped into a coin cell and subjected to the AC impedance measurement. For the room-temperature ionic conductivity measurement, three coin cells for each sample were prepared and measured.

Characterizations. ^{1}H NMR spectra were obtained on a Varian Mercury 400 MHz NMR spectrometer using $CDCl_3$ as the solvent, and the chemical shift was referenced to the residual $CHCl_3$ (7.26 ppm).

ATR-FTIR spectra were recorded using a Nicolet iS50 with a diamond attenuated total reflectance attachment. The thin film samples were placed directly on the sample stage and measured.

TGA and DSC analyses were performed on a TA Instrument Q5500 and TA Instrument Q2000, respectively. In the DSC measurement, the sample was cooled to −80 °C and then heated to 100 °C at a ramping rate of 10 °C/min.

Electrochemical impedance spectroscopy (EIS) was measured on a Biologic VSP300 potentiostat station coupled with an ESPEC BTU-133 benchtop temperature chamber at the frequency range of 7 MHz to 100 mHz.

The tensile test was performed on an Instron 5565 tension tester at an extension rate of 50 mm/min. Vitrimer electrolyte samples were cut into strips and subjected to the tensile test.

The stress−relaxation studies at variable temperatures were performed using a TA ARES-G2 rheometer coupled with a Smart Swap Advanced Peltier System (APS) Jacket and Environmental Control Box. Vitrimer electrolyte films with a thickness of 1 cm were obtained using a hot pressing method, and the disc samples with a diameter of 8 mm were obtained using a 5/16 in. cylinder puncher.

RESULTS AND DISCUSSION

Our synthetic route is shown in Figure 1b. We focused on the PEO chain with M_n = 2000 (degree of polymerization, DP,

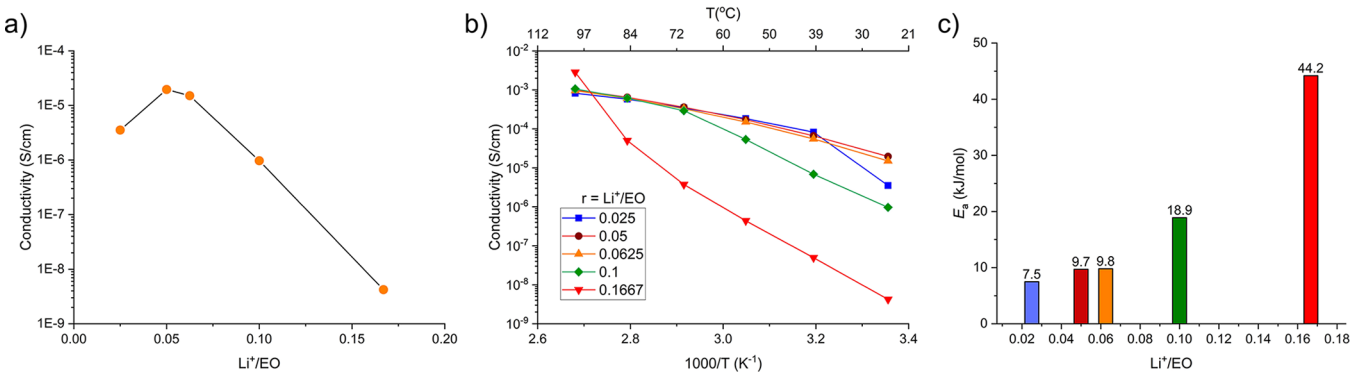

Figure 2. (a) Room-temperature and (b) temperature-dependent ionic conductivity of **VE1-5** at various Li^+/EO ratios. (c) Activation energy of ion conduction for **VE1-5** with various Li^+/EO ratios were retrieved from the VTF model analyses. Note: the activation energies for Li^+/EO = 0.1 and 0.167 were obtained in the temperature range below the melting point and that for Li^+/EO = 0.025 was obtained above the melting point.

equals 45), as it has been previously demonstrated that increasing the DP of network strands can improve the segmental motion and corresponding ionic conductivity and that this trend starts to plateau at DP = 45 for the PEO polymer.[32] The chain ends of PEO polymer were functionalized into acetoacetates through transesterification in the presence of an excess amount of *tert*-butyl acetoacetate. The conversion was monitored by ^{1}H NMR (Figure S1), and the excess *tert*-butyl acetoacetate was removed by vacuum distillation. Subsequent one-pot curing with lithium bis(fluorosulfonyl)imide (LiFSI) using an amine cross-linker yielded the target vitrimer electrolyte (VE). The successful network formation was evidenced by Fourier transform infrared (FTIR) spectra, where the 1743 and 1715 cm^{-1} peaks corresponding to acetoacetate ester and ketone groups vanished after the curing process and new peaks associated with the double bond and ester of the dynamic bonds appeared at 1646 and 1597 cm^{-1} (Figure S2), respectively, in agreement with a previous report.[28]

The molar ratio of the lithium salt to ethylene oxide repeating unit (Li^+/EO) in **VE1-5** was optimized to achieve high ionic conductivity. We observed that the impact of the Li^+/EO ratio on ionic conductivity was significant (Figure 2a) and was consistent with previous observations for PEO based network electrolyte,[32,33] where the ionic conductivity initially increased and then reduced over the Li^+/EO range of 0.025−0.167. The initial increase was ascribed to the suppression of crystallinity and increased salt concentration, while the drop after Li^+/EO = 0.0625 has been attributed to the Li^+ ion induced interchain complexation that immobilize the polymer strands. The formation of complexes was corroborated by differential scanning calorimetry (DSC) results, in which new endothermic peaks corresponding to melting of the Li^+ complex appear at 75 and 92 °C for Li^+/EO = 0.1 and 0.167, respectively (Figure S6). We note that a further increase in the Li^+/EO ratio either led to incomplete dissolution of the LiFSI salt (Li^+/EO = 0.25) or yielded not fully cured mixtures (Li^+/EO = 0.5 or 1). The latter observation could be due to the burial of polymer chains in the salt matrix that impeded the network formation. Collectively, the **VE1-5** with Li^+/EO = 0.0625 showed no crystalline features and afforded an optimal room-temperature ionic conductivity of ~10^{-5} S/cm, which is comparable to previously reported values for PEO based polymer electrolytes.[34−39]

As for a comparison, a liner PEO with methyl ether chain-end-capping groups (mPEO, M_n = 2000) was studied to elucidate the impact of the network formation strategy. In striking contrast, the crystallinity of mPEO cannot be effectively suppressed in the Li^+/EO range of 0.025−0.1. All samples showed a strong crystalline feature with a melting point of around 35−40 °C (Figure S8). Notably, the complexation of mPEO at a ratio of Li^+/EO = 6 possesses a higher melting point than **VE1-5** (114 °C vs 92 °C). This observation is also in contrast to previous reports, in which a high molecular weight PEO (M_w = 5 000 000) was investigated as an electrolyte matrix,[33,40] and could be ascribed to the enhanced crystallization and complexation abilities associated with more chain freedom in a low molecular weight PEO polymer. The high molecular weight PEO has less chain freedom due to chain entanglement, and the cross-linked **VE1-5** has infinite molecular weight and junctions that limit the chain motion. The room-temperature ionic conductivity of mPEO electrolytes could not be well characterized due to the poor interfacial contact related to the crystalline feature. We then proceeded to study the conductivity at 70 °C, which is above the melting temperature for Li^+/EO = 0.025−0.1. The ionic conductivity and its evolution trend over the Li^+/EO ratio agree well with that of **VE1-5** (Figure S10).

Next, we examined the temperature-dependent ionic conductivity behavior of **VE1-5**. As shown in Figure 2b, the **VE1-5** with Li^+/EO = 0.05 and 0.0625 yielded a trend that can be well fitted with the Vogel−Tamman−Fulcher (VTF) model (eq 1),[41] which describes the segmental motion-coupled ion transport in polymer electrolyte (Figure S9). The calculated activation energy of ion transportation for Li^+/EO = 0.05 and 0.0625 are 9.7 and 9.8 kJ/mol, respectively (Figure 2c), consistent with reported values for polyether-based electrolytes.[32,42] On the other hand, the dependence of ionic conductivity on temperature for Li^+/EO = 0.025, 0.1, and 0.167 showed a change in slope in the investigated temperature range (Figure S9). This can be due to either crystallization or complexation below a certain temperature, as evidenced by the consistency between the observed transition temperatures and melting points from DSC results (Figure S6). As a result, a higher activation energy was obtained from the VTF fitting analysis (18.9 kJ/mol for Li^+/EO = 0.1 and 44.2 kJ/mol for Li^+/EO = 0.167, Figure 2c). Interestingly, once the temperature exceeded the melting transition (33 °C for Li^+/EO = 0.025 and 75 °C for Li^+/EO = 0.1), a similar dependence was observed, suggesting the same segmental motion dominated the ion transport mechanism (in the absence of other limiting factors). The **VE1-5** with Li^+/EO = 0.0625 showed completed

suppression of crystallinity and gave the maximum ionic conductivity. Therefore, it was of great interest and was selected for further characterization.

$$\sigma = A \exp\left[-\frac{E_a}{R(T - T_0)}\right] \quad (1)$$

We further evaluated the electrochemical stability window of **VE1-5** to demonstrate the feasibility as a solid electrolyte for the lithium metal battery. The anodic and cathodic stabilities of **VE1-5** were characterized separately through the cyclic voltammetry (CV) tests of Li/**VE1-5**/steel cells. The CV curve of the anodic stability test (up to 5.0 V vs Li^+/Li) showed a characteristic oxidation potential onset of 4.3 V in the first cycle (Figure S11). Along with the gradual drop in overall current, a shift toward a higher voltage value (4.8 V) in the oxidation potential onset was observed in the following three testing cycles, indicating the formation of a passivation interface that prevents further side reactions. Meanwhile, the CV curve of the cathodic stability test (up to −0.3 V vs Li^+/Li) indicated two minor reduction peaks (0.88 and 1.21 V) and a shoulder peak (1.32 V) (Figure S11). In agreement with a previous report,[40] the peak at 0.88 V is associated with reversible species on the electrode surface (e.g., oxide), as suggested by a paring anodic peak at 0.98 V and high reversibility in the following three cycles. In contrast, the peak at 1.21 V and shoulder peak at 1.32 V disappeared in the following cycles, implying the side reaction of **VE1-5**. Nevertheless, the formation of a passivation layer blocks any further reaction with the electrolyte. Therefore, our **VE1-5** possesses an electrochemical stability similar to that of conventional PEO-based polymer electrolytes and is suitable for lithium metal batteries.

To demonstrate the reprocessability and recyclability of prepared VE, a hot-press experiment was performed. As seen in Figure 3a, the **VE1-5** pieces can be successfully reprocessed into a homogeneous film after compression at 90 °C for 30 min. The retention of ionic conductivity was confirmed by the impedance measurement, which yielded an ionic conductivity of $\sim 10^{-5}$ S/cm, a value similar to that of pristine VE. The highly recyclable nature of the VE was further illustrated by seven times of reprocessing, after which the ionic conductivity remained nearly unchanged (Figure 3b). Meanwhile, the mechanical properties of **VE1-5** before and after recycling were measured to evaluate the feasibility of being applied as a separator. A typical curve obtained from the tensile test of **VE1-5** is shown in Figure 3c. The pristine elastic and free-standing electrolyte (see SI Movie for further details) possessed a Young's modulus of 1.05 ± 0.10 MPa, break strain of 367 ± 5%, tensile strength of 1.18 ± 0.10 MPa, and toughness of 2.48 ± 0.19 MPa, indicating good mechanical durability and the feasibility for a electrode insulator. While the stress−strain curves of recycled VE indicated considerable deterioration in mechanical properties (Young's modulus of 0.23 ± 0.02 MPa and toughness of 0.72 ± 0.10 MPa), the recycled VE is still mechanically robust enough to be used as a separator (Table S3). The reduction in mechanical performance postrecycling could be attributed to the lithium cation catalyzed side reaction (e.g., amine−ester transamination) that diminishes the network integrity. The role of the lithium cation as a Lewis acid catalyst will also be discussed in the following section. Despite the decrease in modulus, the ionic conductivity remains unchanged after recycling, which could

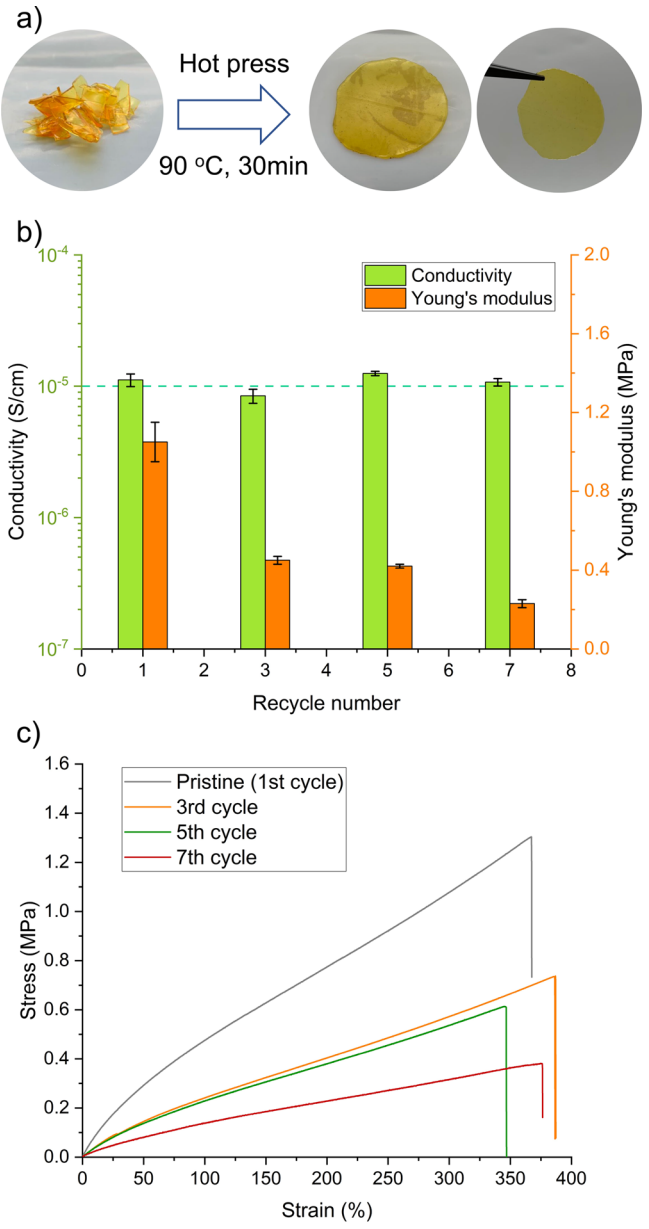

Figure 3. (a) Hot-press reprocessing of **VE1-5** pieces into a homogeneous film. (b) Ionic conductivity of **VE1-5** after different times of reprocessing. The dashed line indicates the conductivity of 10^{-5} S/cm. (c) Representative stress−strain curve of **VE1-5**. The pristine film was obtained after the first hot press cycle of the cured electrolyte network.

be explained by the unchanged T_g of the recycled polymer network as the ion conduction is coupled to the chain segmental motion (Figure S7).

The recyclability of VE originated from the dynamic exchange of polymer strands associated with embedded dynamic vinylogous urethane bonds. To quantitatively evaluate the dynamics and, therefore, recyclability, stress−relaxation characterization was conducted in the temperature range of 90−110 °C. This range was chosen to avoid potential isothermal decomposition of LiFSI salt that occurs at >110 °C.[43] As shown in Figure 4a, a complete stress dissipation was observed within 10^2−10^3 s, and analysis through the Maxwell model (eq 2) indicated that VE relaxed significantly faster than the plain vitrimer network (Figure 4b).

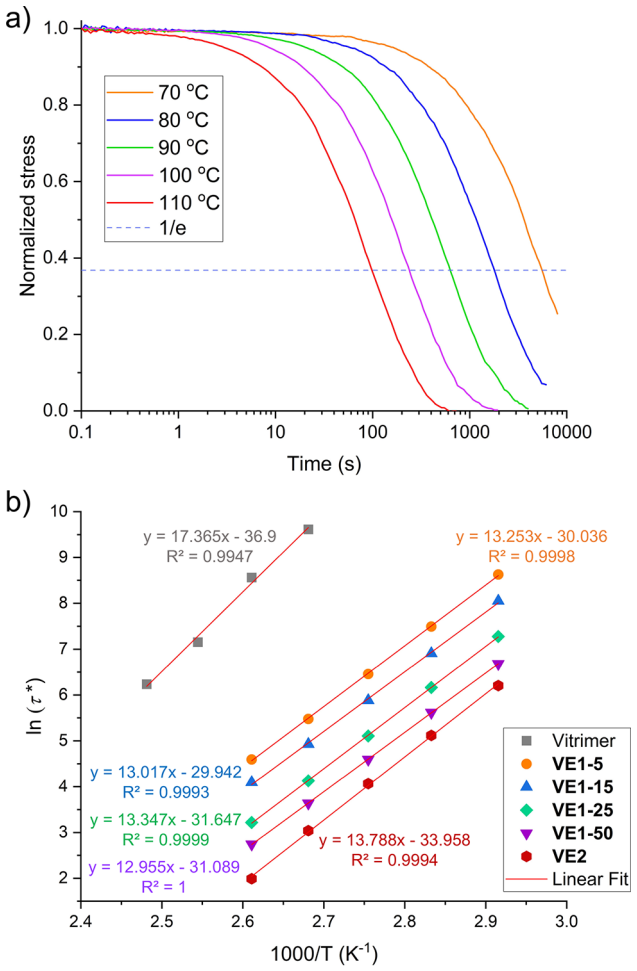

Figure 4. (a) Stress–relaxation curves of **VE1-5** at various temperatures. (b) Arrhenius analysis of the characteristic relaxation time against the inversed temperature.

$$G = G_0 \exp\left(-\frac{t}{\tau^*}\right) \tag{2}$$

$$\tau^* = \tau_0 \exp\left(-\frac{E_a}{RT}\right) \tag{3}$$

Further Arrhenius analysis using eq 3 provided an activation energy E_a of 111 and 144 kJ/mol for the VE and plain vitrimer, respectively. The lower E_a value of VE suggested a different exchange mechanism in VE. We attributed this enhanced dynamic exchange to the presence of LiFSI in the matrix, which acts as a Lewis acid catalyst and may have promoted the dynamic exchange of vinylogous urethane, which was also seen in a previous study.[44]

The reprocessability property associated with network dynamics can be further "tuned" by adjusting the rate of chain/bond exchange. From the reaction standpoint, the rate of chain exchange is dependent on the abundance of vinylogous urethane and amine functionalities in the polymer matrix. Thus, increasing the amount of excess amine could improve the exchange rate (and thus related network dynamics), as previously observed.[45,46] We therefore sought to control the amount of excess amine to tune its reprocessability. Accordingly, VE samples with various amounts of excess amine (**VE1-*x***, where x = 5, 15, 25, and 50 mol % relative to the vinylogous urethane) were prepared and subjected to stress–relaxation characterization to elucidate the exchange dynamics. As expected, a higher amount of excess amine led to a faster network relaxation across the temperature range of study (Figure 4b). Specifically, we observed that **VE1-50** dissipated stress 7 times faster than **VE1-5** at 110 °C (or $1000/T$ = 2.61 K^{-1}). Additionally, Arrhenius fittings were performed for temperature dependence data, and the obtained results consistently yielded similar E_a values of ∼110 kJ/mol, indicating the same exchange mechanism (i.e., Li^+ catalyzed exchange reaction). Alternatively, increasing the abundance of vinylogous urethane in the polymer matrix could also improve the network dynamics. By using a shorter PEO chain (M_n = 400, DP = 9), the abundance of vinylogous urethane in the network was increased by ∼5-fold, and the dynamics was improved by a factor of 14 (Figure 4b). However, this improvement occurred at the expense of low ionic conductivity (8×10^{-9} S/cm for **VE2**) due to the significant drop in segmental motions, i.e., a higher T_g than **VE1-*x*** (Figure S6).

CONCLUSION

In conclusion, direct reprocessing of network electrolyte has been shown through the incorporation of dynamic covalent bonds into the network electrolyte. This was accomplished without detrimentally affecting the electrolyte's mechanical and ionic conducting properties. We expect that the network electrolyte can be formulated for manufacturing procedures, including extrusion, hot press, and roll-to-roll processing. Lastly, our electrolyte is observed to be reprocessed and recycled, indicating its utility toward sustainable all-solid-state batteries.

AUTHOR INFORMATION

Corresponding Author

Zhenan Bao – *Department of Chemical Engineering, Stanford University, Stanford, California 94305, United States;* orcid.org/0000-0002-0972-1715; Email: zbao@stanford.edu

Authors

Yangju Lin – *Department of Chemical Engineering, Stanford University, Stanford, California 94305, United States;* orcid.org/0000-0001-6378-7179

Yuelang Chen – *Department of Chemical Engineering and Department of Chemistry, Stanford University, Stanford, California 94305, United States;* orcid.org/0000-0002-5249-0596

Zhiao Yu – *Department of Chemical Engineering and Department of Chemistry, Stanford University, Stanford, California 94305, United States;* orcid.org/0000-0001-8746-1640

Zhuojun Huang – *Department of Materials Science and Engineering, Stanford University, Stanford, California 94305, United States;* orcid.org/0000-0001-6236-8693

Jian-Cheng Lai − *Department of Chemical Engineering, Stanford University, Stanford, California 94305, United States*

Jeffrey B.-H. Tok − *Department of Chemical Engineering, Stanford University, Stanford, California 94305, United States*

Yi Cui − *Department of Materials Science and Engineering, Stanford University, Stanford, California 94305, United States; Stanford Institute for Materials and Energy Sciences, SLAC National Accelerator Laboratory, Menlo Park, California 94025, United States;* orcid.org/0000-0002-6103-6352

Notes

The authors declare no competing financial interest.

■ ACKNOWLEDGMENTS

The materials design and synthesis of this work were partly supported by Stanford Precourt Pioneering Project - "Reinventing Plastics". The battery testing and characterization were supported by the Assistant Secretary for Energy Efficiency and Renewable Energy, Office of Vehicle Technologies of the U.S. Department of Energy, under the Battery Materials Research (BMR) program. Part of this work was performed at the Stanford Nano Shared Facilities (SNSF), supported by the National Science Foundation under Award ECCS-2026822.

■ REFERENCES

(1) Mauger, A.; Julien, C. M.; Paolella, A.; Armand, M.; Zaghib, K. Building Better Batteries in the Solid State: A Review. *Materials (Basel)* **2019**, *12* (23), 3892.

(2) Zhao, Q.; Stalin, S.; Zhao, C.-Z.; Archer, L. A. Designing Solid-State Electrolytes for Safe, Energy-Dense Batteries. *Nat. Rev. Mater.* **2020**, *5* (3), 229−252.

(3) Lopez, J.; Mackanic, D. G.; Cui, Y.; Bao, Z. N. Designing Polymers for Advanced Battery Chemistries. *Nat. Rev. Mater.* **2019**, *4* (5), 312−330.

(4) Li, J.; Cai, Y.; Wu, H.; Yu, Z.; Yan, X.; Zhang, Q.; Gao, T. Z.; Liu, K.; Jia, X.; Bao, Z. Polymers in Lithium-Ion and Lithium Metal Batteries. *Adv. Energy Mater.* **2021**, *11* (15), 2003239.

(5) Fenton, D. E.; Parker, J. M.; Wright, P. V. Complexes of Alkali Metal Ions with Poly(Ethylene Oxide). *Polymer* **1973**, *14* (11), 589.

(6) Long, L.; Wang, S.; Xiao, M.; Meng, Y. Polymer Electrolytes for Lithium Polymer Batteries. *J. Mater. Chem. A* **2016**, *4* (26), 10038−10069.

(7) Zhang, X.; Daigle, J. C.; Zaghib, K. Comprehensive Review of Polymer Architecture for All-Solid-State Lithium Rechargeable Batteries. *Materials (Basel)* **2020**, *13* (11), 2488.

(8) Wang, J.; Li, S.; Zhao, Q.; Song, C.; Xue, Z. Structure Code for Advanced Polymer Electrolyte in Lithium-Ion Batteries. *Adv. Funct. Mater.* **2021**, *31* (12), 2008208.

(9) Zhou, D.; Shanmukaraj, D.; Tkacheva, A.; Armand, M.; Wang, G. Polymer Electrolytes for Lithium-Based Batteries: Advances and Prospects. *Chem.* **2019**, *5* (9), 2326−2352.

(10) Zhao, W.; Yi, J.; He, P.; Zhou, H. Solid-State Electrolytes for Lithium-Ion Batteries: Fundamentals, Challenges and Perspectives. *Electrochem. Energy Rev.* **2019**, *2* (4), 574−605.

(11) Xue, Z. G.; He, D.; Xie, X. L. Poly(Ethylene Oxide)-Based Electrolytes for Lithium-Ion Batteries. *J. Mater. Chem. A* **2015**, *3* (38), 19218−19253.

(12) Webb, M. A.; Jung, Y.; Pesko, D. M.; Savoie, B. M.; Yamamoto, U.; Coates, G. W.; Balsara, N. P.; Wang, Z. G.; Miller, T. F., 3rd Systematic Computational and Experimental Investigation of Lithium-Ion Transport Mechanisms in Polyester-Based Polymer Electrolytes. *ACS Cent Sci.* **2015**, *1* (4), 198−205.

(13) Fan, L.-Z.; He, H.; Nan, C.-W. Tailoring Inorganic−Polymer Composites for the Mass Production of Solid-State Batteries. *Nat. Rev. Mater.* **2021**, *6* (1), 1003−1019.

(14) Schneiderman, D. K.; Hillmyer, M. A. 50th Anniversary Perspective: There Is a Great Future in Sustainable Polymers. *Macromolecules* **2017**, *50* (10), 3733−3749.

(15) Thompson, D. L.; Hartley, J. M.; Lambert, S. M.; Shiref, M.; Harper, G. D. J.; Kendrick, E.; Anderson, P.; Ryder, K. S.; Gaines, L.; Abbott, A. P. The Importance of Design in Lithium Ion Battery Recycling − a Critical Review. *Green Chem.* **2020**, *22* (22), 7585−7603.

(16) Winne, J. M.; Leibler, L.; Du Prez, F. E. Dynamic Covalent Chemistry in Polymer Networks: A Mechanistic Perspective. *Poly. Chem.* **2019**, *10* (45), 6091−6108.

(17) Scheutz, G. M.; Lessard, J. J.; Sims, M. B.; Sumerlin, B. S. Adaptable Crosslinks in Polymeric Materials: Resolving the Intersection of Thermoplastics and Thermosets. *J. Am. Chem. Soc.* **2019**, *141* (41), 16181−16196.

(18) Podgorski, M.; Fairbanks, B. D.; Kirkpatrick, B. E.; McBride, M.; Martinez, A.; Dobson, A.; Bongiardina, N. J.; Bowman, C. N. Toward Stimuli-Responsive Dynamic Thermosets through Continuous Development and Improvements in Covalent Adaptable Networks (Cans). *Adv. Mater.* **2020**, *32* (20), 1906876.

(19) Jing, B. B.; Evans, C. M. Catalyst-Free Dynamic Networks for Recyclable, Self-Healing Solid Polymer Electrolytes. *J. Am. Chem. Soc.* **2019**, *141* (48), 18932−18937.

(20) Kato, R.; Mirmira, P.; Sookezian, A.; Grocke, G. L.; Patel, S. N.; Rowan, S. J. Ion-Conducting Dynamic Solid Polymer Electrolyte Adhesives. *ACS Macro Lett.* **2020**, *9* (4), 500−506.

(21) Whiteley, J. M.; Taynton, P.; Zhang, W.; Lee, S. H. Ultra-Thin Solid-State Li-Ion Electrolyte Membrane Facilitated by a Self-Healing Polymer Matrix. *Adv. Mater.* **2015**, *27* (43), 6922−7.

(22) Li, S.; Zuo, C.; Zhang, Y.; Wang, J.; Gan, H.; Li, S.; Yu, L.; Zhou, B.; Xue, Z. Covalently Cross-Linked Polymer Stabilized Electrolytes with Self-Healing Performance Via Boronic Ester Bonds. *Poly. Chem.* **2020**, *11* (36), 5893−5902.

(23) Li, S.; Zuo, C.; Jo, Y. H.; Li, S.; Jiang, K.; Yu, L.; Zhang, Y.; Wang, J.; Li, L.; Xue, Z. Enhanced Ionic Conductivity and Mechanical Properties Via Dynamic-Covalent Boroxine Bonds in Solid Polymer Electrolytes. *J. Membr. Sci.* **2020**, *608*, 118218.

(24) Jo, Y. H.; Li, S.; Zuo, C.; Zhang, Y.; Gan, H.; Li, S.; Yu, L.; He, D.; Xie, X.; Xue, Z. Self-Healing Solid Polymer Electrolyte Facilitated by a Dynamic Cross-Linked Polymer Matrix for Lithium-Ion Batteries. *Macromolecules* **2020**, *53* (3), 1024−1032.

(25) Montarnal, D.; Capelot, M.; Tournilhac, F.; Leibler, L. Silica-Like Malleable Materials from Permanent Organic Networks. *Science* **2011**, *334* (6058), 965−968.

(26) Denissen, W.; Winne, J. M.; Du Prez, F. E. Vitrimers: Permanent Organic Networks with Glass-Like Fluidity. *Chem. Sci.* **2016**, *7* (1), 30−38.

(27) Denissen, W.; Rivero, G.; Nicolaÿ, R.; Leibler, L.; Winne, J. M.; Du Prez, F. E. Vinylogous Urethane Vitrimers. *Adv. Funct. Mater.* **2015**, *25* (16), 2451−2457.

(28) Spiesschaert, Y.; Taplan, C.; Stricker, L.; Guerre, M.; Winne, J. M.; Du Prez, F. E. Influence of the Polymer Matrix on the Viscoelastic Behaviour of Vitrimers. *Poly. Chem.* **2020**, *11* (33), 5377−5385.

(29) Lessard, J. J.; Garcia, L. F.; Easterling, C. P.; Sims, M. B.; Bentz, K. C.; Arencibia, S.; Savin, D. A.; Sumerlin, B. S. Catalyst-Free Vitrimers from Vinyl Polymers. *Macromolecules* **2019**, *52* (5), 2105−2111.

(30) Lessard, J. J.; Scheutz, G. M.; Sung, S. H.; Lantz, K. A.; Epps, T. H., 3rd; Sumerlin, B. S. Block Copolymer Vitrimers. *J. Am. Chem. Soc.* **2020**, *142* (1), 283−289.

(31) Ishibashi, J. S. A.; Pierce, I. C.; Chang, A. B.; Zografos, A.; El-Zaatari, B. M.; Fang, Y.; Weigand, S. J.; Bates, F. S.; Kalow, J. A. Mechanical and Structural Consequences of Associative Dynamic

Cross-Linking in Acrylic Diblock Copolymers. *Macromolecules* **2021**, *54* (9), 3972−3986.
(32) Mackanic, D. G.; Michaels, W.; Lee, M.; Feng, D. W.; Lopez, J.; Qin, J.; Cui, Y.; Bao, Z. N. Crosslinked Poly(Tetrahydrofuran) as a Loosely Coordinating Polymer Electrolyte. *Adv. Energy Mater.* **2018**, *8* (25), 1800703.
(33) Sylla, S.; Sanchez, J. Y.; Armand, M. Electrochemical Study of Linear and Crosslinked Poe-Based Polymer Electrolytes. *Electrochim. Acta* **1992**, *37* (9), 1699−1701.
(34) Aihara, Y.; Kuratomi, J.; Bando, T.; Iguchi, T.; Yoshida, H.; Ono, T.; Kuwana, K. Investigation on Solvent-Free Solid Polymer Electrolytes for Advanced Lithium Batteries and Their Performance. *J. Power Sources* **2003**, *114* (1), 96−104.
(35) Pan, Q.; Smith, D. M.; Qi, H.; Wang, S.; Li, C. Y. Hybrid Electrolytes with Controlled Network Structures for Lithium Metal Batteries. *Adv. Mater.* **2015**, *27* (39), 5995−6001.
(36) Ben youcef, H.; Garcia-Calvo, O.; Lago, N.; Devaraj, S.; Armand, M. Cross-Linked Solid Polymer Electrolyte for All-Solid-State Rechargeable Lithium Batteries. *Electrochim. Acta* **2016**, *220*, 587−594.
(37) Tong, Y.; Lyu, H.; Xu, Y.; Prasad Thapaliya, B.; Li, P.; Sun, X.-G.; Dai, S. All-Solid-State Interpenetrating Network Polymer Electrolytes for Long Cycle Life of Lithium Metal Batteries. *J. Mater. Chem. A* **2018**, *6* (30), 14847−14855.
(38) Li, X.; Zheng, Y.; Duan, Y.; Shang, M.; Niu, J.; Li, C. Y. Designing Comb-Chain Crosslinker-Based Solid Polymer Electrolytes for Additive-Free All-Solid-State Lithium Metal Batteries. *Nano Lett.* **2020**, *20* (9), 6914−6921.
(39) Jiang, K.; Wang, J.; Zuo, C.; Li, S.; Li, S.; He, D.; Peng, H.; Xie, X.; Poli, R.; Xue, Z. Facile Fabrication of Polymer Electrolytes Via Lithium Salt-Accelerated Thiol-Michael Addition for Lithium-Ion Batteries. *Macromolecules* **2020**, *53* (17), 7450−7459.
(40) Zhang, H.; Liu, C.; Zheng, L.; Xu, F.; Feng, W.; Li, H.; Huang, X.; Armand, M.; Nie, J.; Zhou, Z. Lithium Bis(Fluorosulfonyl)Imide/Poly(Ethylene Oxide) Polymer Electrolyte. *Electrochim. Acta* **2014**, *133*, 529−538.
(41) Stolwijk, N. A.; Wiencierz, M.; Heddier, C.; Kosters, J. What Can We Learn from Ionic Conductivity Measurements in Polymer Electrolytes? A Case Study on Poly(Ethylene Oxide) (Peo)-Nai and Peo-Litfsi. *J. Phys. Chem. B* **2012**, *116* (10), 3065−74.
(42) Golodnitsky, D.; Strauss, E.; Peled, E.; Greenbaum, S. Review—on Order and Disorder in Polymer Electrolytes. *J. Electrochem. Soc.* **2015**, *162* (14), A2551−A2566.
(43) Kerner, M.; Plylahan, N.; Scheers, J.; Johansson, P. Thermal Stability and Decomposition of Lithium Bis(Fluorosulfonyl)Imide (Lifsi) Salts. *RSC Adv.* **2016**, *6* (28), 23327−23334.
(44) Denissen, W.; Droesbeke, M.; Nicolay, R.; Leibler, L.; Winne, J. M.; Du Prez, F. E. Chemical Control of the Viscoelastic Properties of Vinylogous Urethane Vitrimers. *Nat. Commun.* **2017**, *8*, 14857.
(45) Guerre, M.; Taplan, C.; Nicolay, R.; Winne, J. M.; Du Prez, F. E. Fluorinated Vitrimer Elastomers with a Dual Temperature Response. *J. Am. Chem. Soc.* **2018**, *140* (41), 13272−13284.
(46) Taplan, C.; Guerre, M.; Winne, J. M.; Du Prez, F. E. Fast Processing of Highly Crosslinked, Low-Viscosity Vitrimers. *Mater. Horiz.* **2020**, *7* (1), 104−110.